Iranian Journal of Materials Forming 10 (4) (2023) 4-13

Online ISSN: 2383-0042

IJMF

Iranian Journal of Materials Forming

Journal Homepage: http://ijmf.shirazu.ac.ir

Research Article

Influence of Machining Parameters on the Structural Changes of Bio-Titanium Dental Implants

Sh. Alizadeh[1], M. Shahbaz[1*], M. Kavanlouei[1] and S. Salam Rahimi[2]

[1] Department of Materials Science and Engineering, Faculty of Engineering, Urmia University, Urmia, Iran
[2] Digital dental clinic, Mahabad, Iran

ARTICLE INFO

Article history:

Received 30 September 2023
Reviewed 11 November 2023
Revised 30 December 2023
Accepted 31 January 2024

Keywords:

Ti6Al4V-ELI
Dental implant
Machining
XRD pattern
Texture parameter

Please cite this article as:

Shaghayegh, A., Shahbaz, M., Kavanlouei, M., & Salam Rahimi, S. (2023). Influence of machining parameters on the structural changes of bio-titanium Dental Implants. *Iranian Journal of Materials Forming, 10*(4) 4-13. https://doi.org/10.22099/IJMF.2024.48482.1270

ABSTRACT

This study investigates the impact of machining parameters on the structural changes of dental implants made from bio-titanium alloy (Ti6Al4V-ELI). The implants were designed based on a commercial model and machined under various conditions. The study specifically examines the influence of spindle rotation (S) and cutting depth (Q) on grain size, micro strain, dislocation density, and texture parameter. X-ray diffraction (XRD) was used to analyze the samples, with X'Pert and Maud software utilized to evaluate XRD peak broadening and quantifying α and β phases. The Williamson-Hall method was used to investigate microstructural features such as crystallite size and results showed 153.2, 154.06, 15.72, 77.03, and 22.65 nm for as-received sample A, B, C, and D. The study also examined changes in texture qualitatively by comparing the intensity of the peaks of the XRD pattern. The findings provide valuable insights in order to optimize the manufacturing process of medical implants, contributing to enhanced performance and longevity in a biological environment. According to the results obtained from the XRD pattern of the samples, it can be said that due to the machining process and changing parameters, the peak intensity and position for both phases of the alloy were changed compared with those in the as-received sample. In addition, dislocation density was affected by the machining parameters and the interaction plot was used to investigate the trend of these effects. The different T.P (texture parameter) values (both less than and greater than 1) indicated that the texture was changed as a result of the machining process.

1. Introduction

The performance and longevity of medical implants are of paramount importance in the medical field. These factors are significantly influenced by the manufacturing process employed in the creation of these implants. Despite their many benefits, medical implants are not without their limitations, and there are numerous challenges associated with their design, fabrication, and use [1]. The processing techniques of an engineered

* Corresponding author
E-mail address: mehredads1@gmail.com (M. Shahbaz)
https://doi.org/10.22099/IJMF.2024.48482.1270

implant largely determine its preciseness, surface characteristics, and interactive ability with the adjacent tissue(s) in a particular biological environment [2].

An important step in medical implant manufacturing is the selection of an appropriate biomaterial [3]. Among the various materials utilized for medical implants, the titanium alloy Ti6Al4V-ELI has emerged as a popular choice and is widely used in medical applications due to its superior mechanical properties, excellent strength, osseointegration, biocompatibility, high strength-to-weight ratio, and good corrosion resistance [4-6].

The machining process has a significant impact on the life and quality of implants, especially on permanent bio-implants [7]. The manufacturing process, particularly the machining parameters, plays a pivotal role in determining the overall performance of the implant. Parameters such as cutting speed, feed rate, and depth of cut have a significant influence on the surface integrity, microstructure, and mechanical properties of Ti6Al4V-ELI implants. The mechanical properties of this material strongly depend on the initial condition of the as-received material and processing parameters. These parameters can alter the residual stresses, surface roughness, and microhardness of the implants, thereby affecting their performance in a biological environment. Inappropriate machining parameters may lead to the formation of a rough surface, which could increase the risk of bacterial adhesion and subsequent infection. Therefore, it is crucial to optimize these machining parameters to enhance the performance of Ti6Al4V-ELI implants [2, 4, 8].

During the machining process, residual stress is ineluctably generated and constitutes a significant indicator affecting the quality and performance of the machined workpiece. Particularly, fatigue life, fracture behavior, wear resistance, and corrosion resistance of the machined workpiece are all directly influenced by residual stresses [9]. As a result of the machining process, the microstructure and grain size also changes [10].

X-ray diffraction (XRD) is a powerful, non-destructive characterization tool used to investigate changes in the crystallographic structure of a wide variety of materials. The XRD patterns can provide valuable information about phase transformations, average crystallite size, residual stresses, and texture development in machined implants [11, 12]. By analyzing these XRD patterns, one can gain insights into the effects of machining parameters on the microstructural evolution and mechanical performance of Ti6Al4V-ELI implants.

Previous studies have demonstrated that XRD can effectively detect phase transformations in Ti6Al4V-ELI induced by machining. For instance, the transformation of the alpha phase to the beta phase due to high cutting temperatures can be identified from shifts in diffraction peaks. The presence of the beta phase could enhance the hardness and wear resistance of the implants but may also increase their susceptibility to corrosion. Therefore, XRD patterns can provide critical information for optimizing machining parameters to balance mechanical properties and corrosion resistance of Ti6Al4V-ELI implants [13, 14].

In addition to phase transformations, residual stresses induced by machining can also be evaluated using XRD. High residual stresses may lead to distortion and premature failure of implants. The XRD patterns can reveal the distribution and magnitude of residual stresses in machined implants, which can guide adjustments to machining parameters to minimize these residual stresses [9, 15].

The investigation into how machining parameters affect the performance of Ti6Al4V-ELI implants using XRD patterns is a promising approach that can optimize the manufacturing process of medical implants. The insights gained from XRD analysis can guide the selection of appropriate machining parameters to enhance the surface integrity, microstructure, and mechanical properties of implants. This ultimately improves their performance and longevity in a biological environment. The forthcoming sections of this paper will delve into specific methods used in this investigation, present results obtained, and discuss implications for future research.

2. Experimental Procedure

The subject samples of the study are dental implants made from cylindrical shaped bio-titanium alloy (Ti6Al4V-ELI). These implants were designed based on a commercial model and were machined under various machining conditions (Table 1) using CNC machine (11-axis Tornos CNC milling machine). The purpose was to examine the impact of changes in machining parameters, specifically spindle rotation (S) and cutting depth (Q), on the structural changes of the implants (grain size, micro strain, dislocation density, and texture parameter). Fig. 1 shows images of the implants. The chemical composition of the samples in terms of weight percentage of elements is listed in Table 2. The samples were analyzed using an X-ray Diffraction (XRD, PHILIPS-PW1730, copper target with λ=1.5406 Å) device with a time per stage of 0.4 seconds and a step size of 0.04 degrees. X'Pert and Maud software were used for evaluating XRD peak broadening and quantifying α and β phases.

To investigate microstructural features such as crystallite size, various methods are available, among which the Williamson-Hall method is the most common. Contrary to the Debye-Scherrer method, which attributes peak width changes only to grain size, the Williamson-Hall method also examines the effect of lattice strains, considering peak width changes dependent on both grain size and strains present in the lattice. According to the theory presented by Williamson and Hall, as per Eq. 1, the Full Width at Half Maximum (FWHM) of the peak is a function of grain size as well as the strains within the lattice [16].

$$\beta \cos(\theta) = \frac{k\lambda}{D} + 4\varepsilon \sin(\theta) \qquad (1)$$

In Eq. 1, β represents the FWHM (peak width resulting from crystallite size and strains within the lattice), θ is the diffraction angle, k is a constant, λ is the x-ray wavelength, D is the crystallite size, and ε represents the microstrain within the lattice. Using the data extracted from the diffraction pattern and XRD spectrum peaks, one can plot the graph of Eq. 1. In this plot, the slope of the drawn line is equivalent to the lattice strain, and the y-intercept is equivalent to the crystallite size.

The changes in texture were examined qualitatively by comparing the intensity of the peaks of the XRD pattern. Eq. 2 [17] was used to show the degree of changes in the crystal texture of the metal due to plastic deformation.

$$T.P. = \frac{(\frac{I_{hkl}}{I^0_{hkl}})}{\frac{1}{n}\sum_1^n(\frac{I_{hkl}}{I^0_{hkl}})} \qquad (2)$$

where I^0_{hkl} is the intensity of the reference peak and I_{hkl} is the intensity of the deformed sample. The value of T.P equals one, means that no changes have been made to the crystalline texture of the material caused by deformation, and the greater difference in T.P calculated from 1 means more changes have been made in the crystalline texture [17].

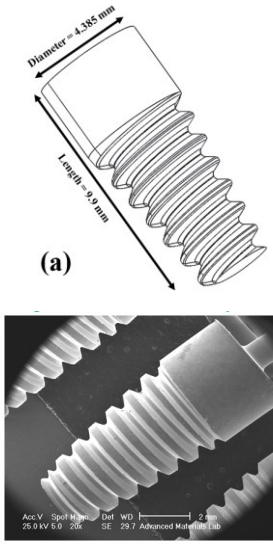

Fig. 1. a) 3D image of designed implant using SolidWorks software, b) SEM (Scanning Electron Microscopy) image of the machined implant.

Table 1. Machining parameters

Sample	Spindle rotation speed (S) (rpm)	Depth of cutting (Q) (mm)
A	1000	0.01
B	1000	0.12
C	500	0.01
D	500	0.12

Table 2. Chemical composition of the samples in terms of the weight percentage of elements

Al	V	Cr	Cu	Fe	Mn	Mo	Nb	Sn	Ni	Si	Zr	Pd	Ru	Ti
6.06	4.40	<0.005	<0.005	0.10	<0.005	<0.01	<0.005	<0.02	<0.005	0.06	0.02	<0.01	<0.01	Base

3. Results and Discussion

Fig. 2 presents the XRD patterns of the machined implants. The XRD patterns encompass the peaks of the primary α and β phases. The XRD patterns of the samples showed proper alignment with the standard JCPDS (Joint Committee on Powder Diffraction Standards) pattern 96-901-6191. According to the results obtained from the XRD pattern of the samples, it can be said that due to the machining process and a change in the parameters, the peak intensity of the β phase was decreased in all four studied samples compared to the as-received sample, and in samples A and C, the peak intensity was decreased significantly (from 115.16 to 40.8 and 42.23, respectively). Additionally, the position of the peaks compared to the as-received sample was slightly changed and the peaks were shifted to the left.

The peaks of the α phase for samples A, and C possess lower intensity than those in the as-received sample and the peak positions were altered compared to the peaks of the as-received Ti-6Al-4V sample. However, the intensity of α phase for samples B, and D did not indicate any significant changes.

In this study, the values for crystallite size and microstrain were calculated for an as-received sample and four manufactured implants under the machining conditions listed in Table 1, using the Williamson-Hall method. For this purpose, the FWHM values for each sample were calculated using the X'Pert software. Instrumental broadening was also considered to enhance the accuracy of the calculations. For simplicity in the calculations, the constant k was approximately considered equal to 1 (Eq. (1)). The plot of (β cos θ) against (sin θ) for the three sharpest peaks of each sample was drawn, and calculations were performed. Fig. 3 shows the Williamson-Hall plot for each sample. The crystallite size and microstrain obtained from the above method for the samples, as well as the volumetric fraction of the samples' phases, which were obtained using the Maud software, are presented in Table 3.

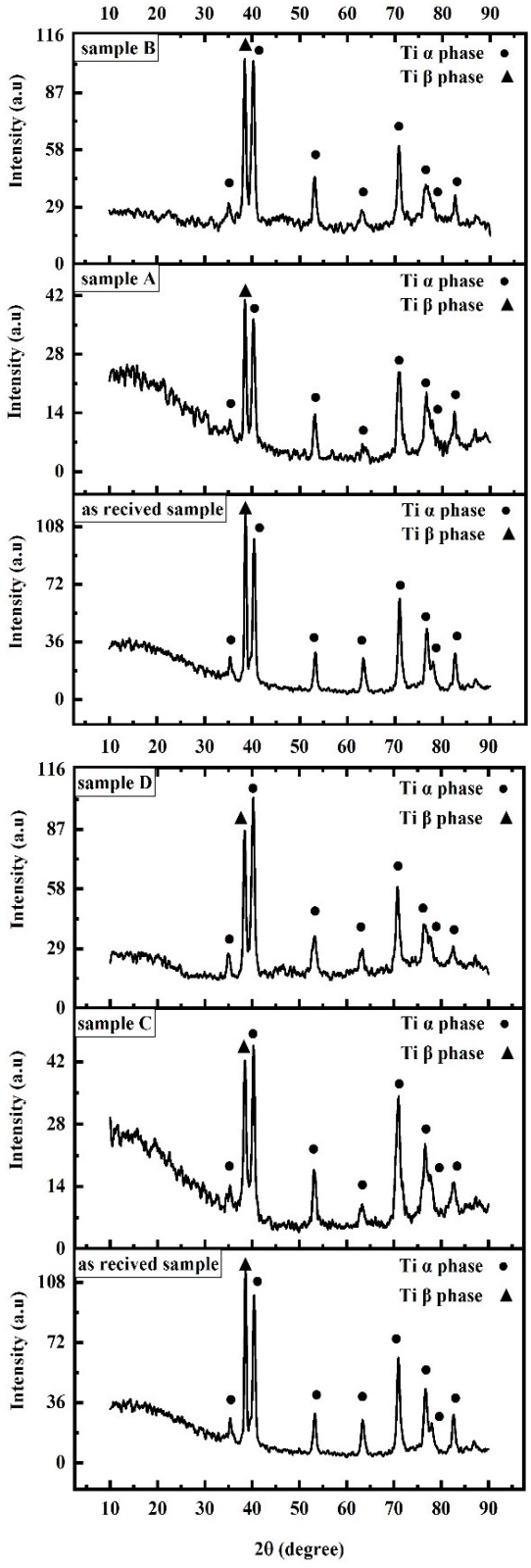

Fig. 2. XRD patterns of as-received, A, B, C, and D samples.

Table 1. Williamson-Hall analysis results

sample	As-received sample	A	B	C	D
Crystallite size (nm)	153.2	154.1	15.72	77	22.7
Micro strain	0.118	0.006	1E-04	0.01	0
α phase (%vol.)	82.48	66.97	68.06	63.9	65.2
β phase (%vol.)	17.52	33.02	31.93	36.1	34.8

Samples A (1000 rpm) and B (1000 rpm) were subjected to different cutting depths, and the subsequent effects on their material properties were analyzed. In terms of crystallite size, Sample A, with a cutting depth of 0.01 mm, exhibited a crystallite size of 154.06 nm, while Sample B, with a larger cutting depth of 0.12 mm, displayed a significantly smaller crystallite size of 15.72 nm. These findings indicate that the increase in cutting depth while maintaining a constant spindle speed of 1000 rpm, had a profound impact on the crystallite size. Sample B, with the deeper cut, demonstrated a substantial reduction in crystallite size compared to the as-received sample, signifying a pronounced grain refinement effect.

Moving on to the evaluation of microstrain, sample A, machined with a cutting depth of 0.01 mm, presented a microstrain of 0.006, which was notably lower than the as-received sample's microstrain of 0.118. In contrast, Sample B, with the deeper cutting depth of 0.12 mm, exhibited an even lower macrostrain of 0.0001, indicating a substantial reduction in lattice distortions when compared to the initial material. These observations underscore the fact that increasing the cutting depth while maintaining a constant spindle speed of 1000 rpm contributed significantly to minimizing the lattice distortions within the crystalline structure, thereby enhancing its stability.

Considering the alpha phase percentage, sample A, machined with a cutting depth of 0.01 mm, displayed an alpha phase percentage of 66.97%, which was lower than the as-received sample's alpha phase percentage of 82.48%. Conversely, Sample B, with the larger cutting depth of 0.12 mm, showed a slightly elevated alpha phase percentage of 68.06%. These findings indicate that altering the cutting depth at a constant spindle speed had an impact on the phase composition of the material. In particular, Sample B demonstrated a preference for the alpha phase under these conditions. This suggests that variations in cutting depth can influence the distribution of crystalline phases within the material, with deeper cuts favoring the alpha phase.

In summary, the analysis of Samples A and B reveals that the cutting depth, when adjusted while maintaining a constant spindle speed of 1000 rpm, plays a significant role in altering material properties. It results in notable changes in crystallite size, microstrain, and phase composition. Specifically, deeper cutting depths lead to smaller crystallite sizes, reduced lattice distortions, and a tendency to favor the alpha phase. These findings provide valuable insights into the optimization of machining parameters to achieve the desired material characteristics. Samples C (500 rpm) and D (500 rpm) were subjected to different cutting depths, allowing us to explore the impact of cutting depth while keeping the spindle rotation speed constant at 500 rpm. Analyzing their material properties reveals several key findings:

In terms of crystallite size, Sample C, with a cutting depth of 0.01 mm, exhibited a crystallite size of 77.03 nm, whereas Sample D, with a deeper cutting depth of 0.12 mm, displayed a slightly larger crystallite size of 22.65 nm. By comparing these results with the as-received sample's crystallite size of 153.2 nm, it becomes evident that both Samples C and D showed deviations from the initial crystallite size. However, the changes observed in these samples were less pronounced than those in Samples A and B, which were machined at 1000 rpm. This implies that increasing the cutting depth at a constant spindle speed of 500 rpm had a milder effect on crystallite size compared to the 1000 rpm case.

Moving on to the evaluation of microstrain, both Sample C (0.01 mm) and Sample D (0.12 mm) exhibited similar microstrain values, measured at 0.006 and 0.002, respectively. These values were notably lower than the as-received sample's microstrain value of 0.118. These

results suggest that increasing the cutting depth while maintaining a constant spindle speed of 500 rpm led to a reduction in lattice distortions in both samples, contributing to a more stable crystalline structure. This observation is consistent with the idea that increasing cutting depth can have a positive impact on lattice stability, even at a lower spindle speed.

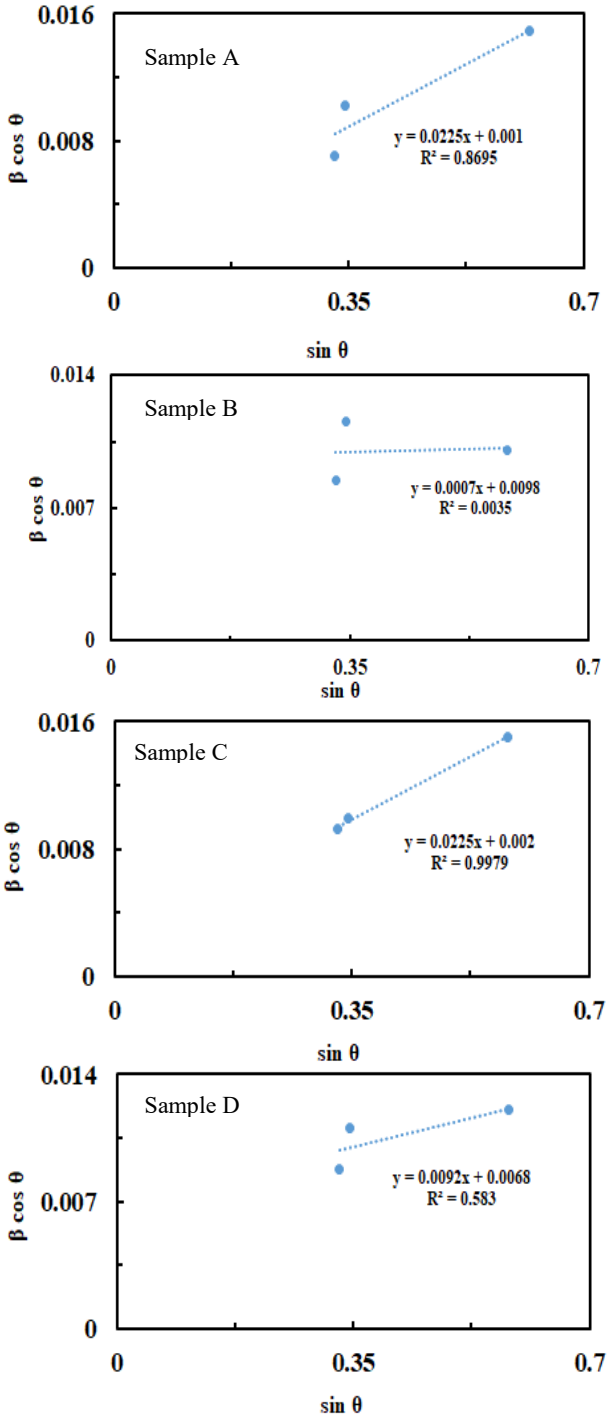

Fig. 3. Williamson Hall diagrams of samples A, B, C and D.

Regarding the alpha phase percentage, Sample C (0.01 mm) had an alpha phase percentage of 63.91%, while Sample D (0.12 mm) had a slightly higher alpha phase percentage of 65.22%. Both Samples C and D exhibited lower alpha phase percentages compared to the as-received sample's alpha phase percentage of 82.48%. These findings suggest that increasing the cutting depth at a constant spindle speed of 500 rpm may lead to a decrease in the alpha phase, similar to what was observed in the 1000 rpm case. However, the effect was not as pronounced, indicating that spindle speed played a more prominent role in influencing the phase composition in such conditions.

In summary, the analysis of Samples C and D demonstrates that varying the cutting depth at a constant spindle speed of 500 rpm has notable effects on material properties, including crystallite size, microstrain, and phase composition. While changes in cutting depth still led to alterations in these properties, the effects were milder compared to the 1000 rpm case. Increasing cutting depth at a lower spindle speed can still contribute to reduced lattice distortions and a more stable crystalline structure, with only a modest impact on phase composition. These findings provide valuable insights for materials processing and optimization.

Samples A and B, machined at 1000 rpm with different cutting depths (0.01 mm and 0.12 mm, respectively), exhibited significant deviations in crystallite size. Sample B, with the deeper cutting depth, displayed a substantial reduction in crystallite size compared to the as-received sample, indicating a pronounced grain refinement effect. In contrast, Samples C and D, machined at 500 rpm with the same cutting depth variations, also showed deviations in crystallite size, but the changes were less pronounced than in the 1000 rpm case. This suggests that there is an interaction between the effects of the two considered machining parameters on the crystallite size (Fig. 4(a)).

In both sets of samples (A and B at 1000 rpm, C and D at 500 rpm), increasing the cutting depth led to a reduction in microstrain. This indicates that deeper cuts, regardless of the spindle speed, contributed to reduced lattice distortions and a more stable crystalline structure.

The reduction in microstrain was more pronounced in Sample B (1000 rpm) with the deeper cut, implying that higher spindle speed combined with increased cutting depth had a more significant effect on lattice stability. This suggests that there is an interaction between the effects of the two considered machining parameters on the microstrain (Fig. 4(b)).

The dislocation density can also be calculated using the parameters derived from Eq. 1, according to Eqs. 3 to 5 [18]:

$$\rho = (\rho_t \times \rho_s)^{1/2} \quad (3)$$

$$\rho_D = \frac{3}{D^2} \quad (4)$$

$$\rho_s = \frac{6\pi\varepsilon^2}{b^2} \quad (5)$$

In Eq. 3, ρ represents the dislocation density, ρ_D the dislocation density due to crystallite size, ρ_s the dislocation density due to microstrain. In Eq. 4, D represents crystallite size, and in Eq. 5, ε is the strain and b is Burger's vector. The dislocation density of the samples, assuming a Burger's vector b = 0.286 nm, was calculated according to Eqs. 3 to 5 and the values are reported in Table 4. Fig. 5 shows the effect of spindle rotation speed at different cutting depth on the dislocation density, which shows the interaction between two machining parameters.

Dislocation density is a critical parameter in the structural characterization of dental implants, and its variations can have implications for the longevity and osseointegration of the implants. In our study, the expression of dislocation density for different samples serves as a crucial indicator of the internal structural changes induced by machining parameters.

The observed differences in dislocation density between samples may correspond to variations in mechanical properties. Previous research has demonstrated that higher dislocation density can influence the mechanical behavior of materials, affecting factors such as hardness and ductility [19]. Therefore, an increased dislocation density in a dental implant might suggest alterations in its mechanical strength, which could impact its resistance to wear and fatigue.

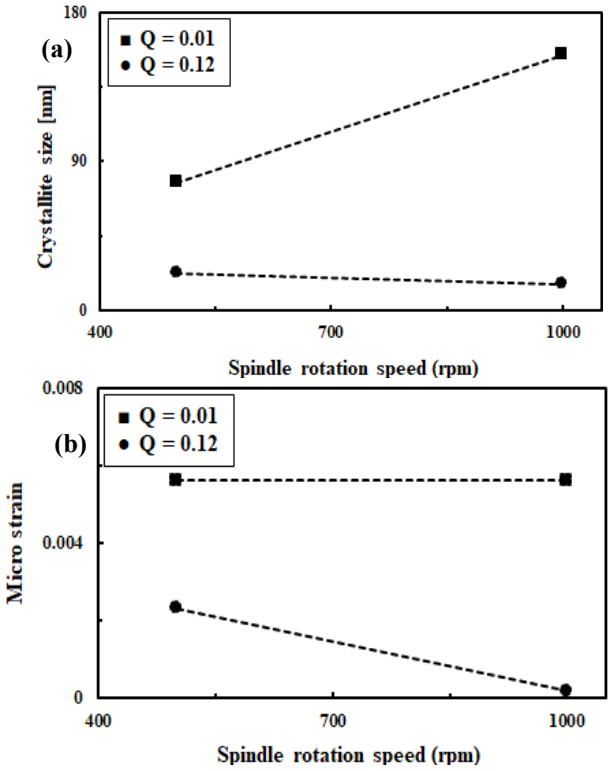

Fig. 4. Interaction plot for machining parameters effects of the crystallite size (a), and microstrain (b).

Table 4. Dislocation density values

Sample	A	B	C	D
Dislocation density	8.34E-05	0.007333	0.001358	0.005077

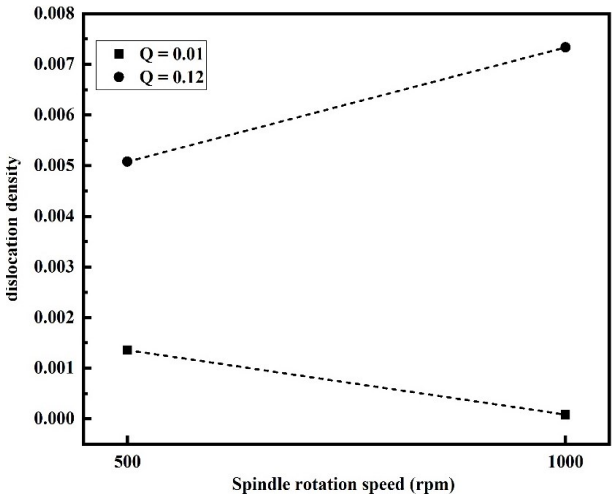

Fig. 5. Interaction plot for machining parameters effects of the dislocation density.

The Longevity in dental implants is often associated with their ability to withstand mechanical stresses over an extended period. If an increase in dislocation density correlates with an increase in mechanical strength, it could potentially lead to an increase in the overall lifespan of the implant. This emphasizes the importance of optimizing machining parameters to adjust dislocation density, ensuring the implant's long-term structural integrity.

Osseointegration, the direct structural and functional connection between the living bone and the surface of a load-bearing implant, is crucial for the success of dental implants. While the direct link between dislocation density and osseointegration may not be well-established in the literature, studies have shown that the surface characteristics and mechanical properties of implants can influence the osseointegration process [20]. Therefore, it is plausible that variations in dislocation density, reflecting changes in the implant's microstructure, may indirectly affect osseointegration by influencing factors such as surface roughness and mechanical stability.

To further elucidate the relationship between dislocation densities and implant performance, future research could incorporate in vitro or in vivo assessments. These studies could evaluate the impact of dislocation density on factors like bacterial adhesion, inflammatory response, and bone-to-implant contact. Exploring these aspects would contribute to a more comprehensive understanding of how structural changes manifest in the functional behavior of dental implants.

Eq. 2 was used to evaluate the texture changes (texture parameter) resulting from the machining process on the samples. A T.P (texture parameter) value of 1 indicates that no changes have occurred in the crystalline texture of the material due to deformation. The more the calculated T.P deviates from 1, the more significant the changes in the crystalline texture are. A sample that did not undergo a machining process (as-received sample) was used as the reference sample. The texture parameter (T.P) was calculated for the peaks identified in Fig. 2. Fig. 6 shows the values of the texture parameter (T.P) for samples A, B, C, and D in different crystallographic planes. According to Fig. 6, the different T.P values (both less than and greater than 1) indicate that the texture has been changed as a result of the machining process.

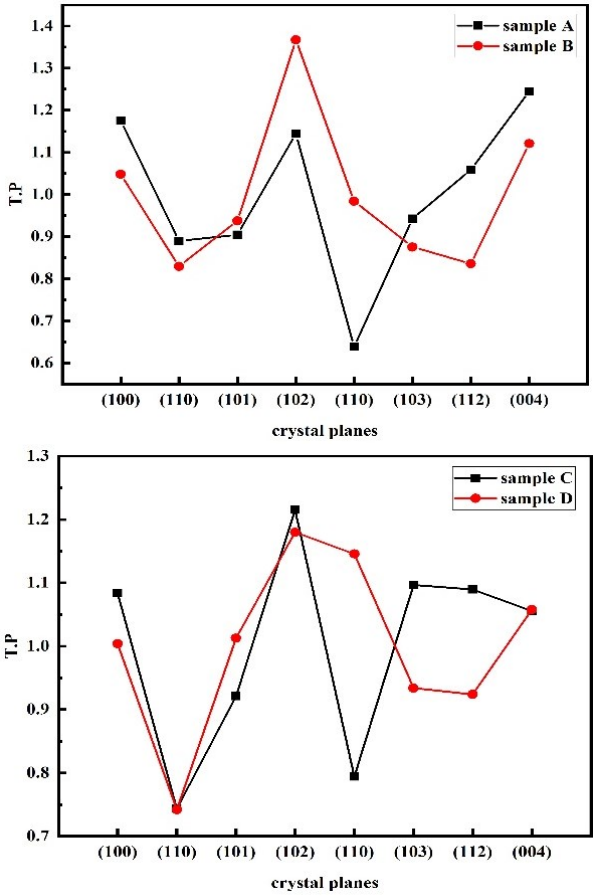

Fig. 6. Texture parameter versus crystal planes for the samples produced by different machining parameters.

4. Conclusion

The study has provided valuable insights into the impact of machining parameters on the structural changes of dental implants made from bio-titanium alloy. The key findings from the study are:

- The machining process and parameter changes led to a decrease in the peak intensity of the β phase in all four studied samples compared to the as-received sample, with significant decreases observed in samples A and C. The peak positions also shifted slightly to the left.
- The intensity of the α phase peaks for samples A and C was lower than that in the as-received sample, and the peak positions were altered.

However, the intensity of the α phase for samples B and D remained almost unchanged.

- Adjusting the cutting depth while maintaining a constant spindle speed significantly alters the material properties, including crystallite size, microstrain, and phase composition. Specifically, deeper cuts result in smaller crystallite sizes, reduced lattice distortions, and a preference for the alpha phase.
- Both sets of samples (A and B at 1000 rpm, C and D at 500 rpm) showed that increasing the cutting depth led to reduced lattice distortions and a more stable crystalline structure. However, the reduction in microstrain was more pronounced at higher spindle speeds.
- These findings suggest that there is an interaction between the spindle speed and cutting depth on both crystallite size and microstrain, with higher spindle speeds and deeper cuts having more significant effects. Moreover, increasing the cutting depth at a constant spindle speed led to a reduction in lattice distortions and a decrease in the alpha phase. This suggests that spindle speed plays a prominent role in influencing phase composition.

In conclusion, this study provides valuable insights into how machining parameters can be optimized to achieve desired material characteristics. The findings highlight the importance of considering both spindle speed and cutting depth when machining bio-titanium dental implants. Further research is needed to fully understand these interactions and their implications for implant performance and longevity.

Acknowledments

The authors are deeply grateful to all those who played a role in the success of this research.

Conflict of Interests

The authors declare no conflict of interest in this research.

Funding

The authors declare that no funds, grants, or other support were received during the preparation of this manuscript.

5. References

[1] Ramezani, M., & Ripin, Z. M. (2023). An overview of enhancing the performance of medical implants with nanocomposites. *Journal of Composites Science*, *7*(5), 199. https://doi.org/10.3390/jcs7050199

[2] Davis, R., Singh, A., Jackson, M. J., Coelho, R. T., Prakash, D., Charalambous, C. P., Ahmed, W., Ribeiro da Silva, L. R., & Lawrence, A. A. (2022). A comprehensive review on metallic implant biomaterials and their subtractive manufacturing. *The International Journal of Advanced Manufacturing Technology*, *120*(3), 1473-1530. https://doi.org/10.1007/s00170-022-08770-8

[3] Pandey, A., & Sahoo, S. (2023). Progress on medical implant: a review and prospects. *Journal of Bionic Engineering*, *20*(2), 470-494. https://doi.org/10.1007/s42235-022-00284-z

[4] Rodriguez, G. M., Bowen, J., Zelzer, M., & Stamboulis, A. (2020). Selective modification of Ti6Al4V surfaces for biomedical applications. *RSC advances*, *10*(30), 17642-17652. https://doi.org/10.1039/C9RA11000C

[5] Balasubramanian Gayathri, Y. K., Kumar, R. L., Ramalingam, V. V., Priyadharshini, G. S., Kumar, K. S., & Prabhu, T. R. (2022). Additive manufacturing of Ti-6Al-4V alloy for biomedical applications. *Journal of Bio-and Tribo-Corrosion*, *8*(4), 98. https://doi.org/10.1007/s40735-022-00700-1

[6] Gheshlaghi, H., Alimirzaloo, V., Shahbaz, M., & Amiri, A. (2023). Finite Element Analysis of Phase Distribution in Forging of the Two-Phase Ti-6Al-4V Alloy to have a Hip Joint Implant. *Iranian Journal of Materials Forming, 9*(4), 26-33. https://doi.org/10.22099/IJMF.2022.44610.1238

[7] Umar Farooq, M., Pervez Mughal, M., Ahmed, N., Ahmad Mufti, N., Al-Ahmari, A. M., & He, Y. (2020). On the investigation of surface integrity of Ti6Al4V ELI using Si-mixed electric discharge machining. *Materials*, *13*(7), 1549. https://doi.org/10.3390/ma13071549

[8] Gheshlaghi, H., Alimirzaloo, V., Shahbaz, M., & Amiri, A. (2022). Numerical study and optimization of the thermomechanical procedure in forging of two-phase Ti-6Al-4V Alloy for artificial hip joint implant. *Iranian*

Journal of Materials Forming, *9*(3), 31-43. https://doi.org/10.22099/IJMF.2022.43334.1219

[9] Wan, M., Ye, X. Y., Wen, D. Y., & Zhang, W. H. (2019). Modeling of machining-induced residual stresses. *Journal of materials science*, *54*, 1-35. https://doi.org/10.1007/s10853-018-2808-0

[10] Rinaldi, S., Rotella, G., & Del Prete, A. (2021). A physically based constitutive model of microstructural evolution of Ti6Al4V hard machining under different lubri-cooling conditions. *The International Journal of Advanced Manufacturing Technology*, *112*, 1641-1659. https://doi.org/10.1007/s00170-020-06540-y

[11] Ali, A., Chiang, Y. W., & Santos, R. M. (2022). X-ray diffraction techniques for mineral characterization: A review for engineers of the fundamentals, applications, and research directions. *Minerals*, *12*(2), 205. https://doi.org/10.3390/min12020205

[12] Qazi, J. I., Rahim, J. S. A. M., Fores, F. H., Senkov, O. N., & Genc, A. (2001). Phase transformations in Ti-6Al-4V-x H alloys. *Metallurgical and Materials Transactions A*, *32*, 2453-2463. https://doi.org/10.1007/s11661-001-0035-8

[13] Wang, P., Chen, F. H., Eckert, J., Pilz, S., Scudino, S., & Prashanth, K. G. (2021). Microstructural evolution and mechanical properties of selective laser melted Ti-6Al-4V induced by annealing treatment. *Journal of Central South University*, *28*(4), 1068-1077. https://doi.org/10.1007/s11771-021-4680-3

[14] Outeiro, J. (2018). Residual stresses in machining operations. *CIRP Encyclopedia of Production Engineering; Laperrière, L., Reinhart, G., Eds*, 1-13. https://doi.org/10.1007/978-3-642-35950-7_16811-1

[15] Mote, V. D., Purushotham, Y., & Dole, B. N. (2012). Williamson-Hall analysis in estimation of lattice strain in nanometer-sized ZnO particles. *Journal of theoretical and applied physics*, *6*, 1-8. https://doi.org/10.1186/2251-7235-6-6

[16] Abbasi, M., Ahmadi, F., & Farzin, M. (2021). Production of ultrafine-grained titanium with suitable properties for dental implant applications by RS-ECAP process. *Metals and Materials International*, *27*, 705-716. https://doi.org/10.1007/s12540-020-00796-5

[17] Farshidi, M. H., Kazeminezhad, M., & Miyamoto, H. (2013). On the natural aging behavior of Aluminum 6061 alloy after severe plastic deformation. *Materials Science and Engineering: A*, *580*, 202-208. https://doi.org/10.1016/j.msea.2013.05.051

[18] Lütjering, G. E. R. D. (1998). Influence of processing on microstructure and mechanical properties of (α+ β) titanium alloys. *Materials Science and Engineering: A*, *243*(1-2), 32-45. https://doi.org/10.1016/S0921-5093(97)00778-8

[19] Matos, G. R. M. (2021). Surface roughness of dental implant and osseointegration. *Journal of Maxillofacial and Oral Surgery*, *20*, 1-4. https://doi.org/10.1007/s12663-020-01437-5